Multiple scattering in the Compton effect. I. Analytic treatment of angular distributions and total scattering probabilities

Anthony C. Tanner and Irving R. Epstein*

Department of Chemistry, Brandeis University, Waltham, Massachusetts 02154
(Received 18 August 1975; revised manuscript received 6 October 1975)

The probabilities of single and multiple Compton scattering and the angular distributions of scattered photons are analyzed in terms of the effects of sample geometry and details of the photon-electron interaction (form of the single-electron cross section). It is shown that the desired quantities may be calculated analytically if Thomson scattering and an appropriate geometry are assumed. Consideration of scattering using an isotropic cross section suggests that in most cases sample geometry is more important than the form of the cross section in determining the probability and angular distribution of single and multiple scattering.

I. INTRODUCTION

When a high-energy photon is inelastically scattered by an electron, the change in wavelength of the scattered photon is determined by the scattering angle θ and the projection p_z of the electron's initial momentum along the scattering vector:

$$\Delta\lambda = \lambda_1 - \lambda_0 = \frac{2h}{mc}\sin^2\tfrac{1}{2}\theta + 2\left(\frac{p_z}{mc}\right)\lambda_0\sin\tfrac{1}{2}\theta, \quad (1)$$

where λ_0 and λ_1 are the initial and final wavelengths, respectively, of the photon. At a fixed scattering angle, then, the energy or wavelength spectrum of scattered radiation (the Compton profile) provides a direct determination of the projection of the electronic momentum distribution of the scattering material on the scattering direction.

A marked revival of interest in the Compton effect has occurred in the past decade, owing to and resulting in advances in both theory and experiment.[1] Recent work, including an international project aimed at standardizing and evaluating Compton techniques,[2] has indicated that perhaps the major outstanding problem in Compton scattering is that of multiple scattering, i.e., successive scatterings of a single photon by more than one electron. The effects of multiple scattering on the Compton profile may be seen by considering the following example of double scattering.

A photon of wavelength λ_0 is scattered at an angle θ_1 by an electron with momentum $\vec{p}_1$ and then again at an angle θ_2 by a second electron with momentum $\vec{p}_2$. The photon is then observed at some angle θ_p (see Fig. 1). The wavelength after the first scattering is λ_1; after the second scattering it is λ_2.

Two applications of Eq. (1) yield, for the observed change in wavelength,

$$\Delta\lambda = \lambda_2 - \lambda_0$$

$$= (2h/mc)(\sin^2\tfrac{1}{2}\theta_1 + \sin^2\tfrac{1}{2}\theta_2)$$

$$+ 2(1/mc)(p_{z1}\lambda_0\sin\tfrac{1}{2}\theta_1 + p_{z2}\lambda_1\sin\tfrac{1}{2}\theta_2).$$

Only the over-all scattering angle θ_p can be measured, and thus the components of the electronic momenta p_{z1} and p_{z2} cannot be inferred from $\Delta\lambda$, since θ_1 and θ_2 are unknown. As may be seen from Fig. 1, many different pairs of individual angles θ_1 and θ_2 may result in a single observed angle θ_p. It is clear that if a significant fraction of photons are multiply scattered, then considerable inaccuracy will result if one attempts to derive the electronic momentum distribution from a measured Compton profile using the assumption of pure single scattering [Eq. (1)].

In order to account for the effects of multiple scattering in a Compton profile measurement, the following two questions must be answered: (a) To what extent are multiply scattered photons being observed? (b) How do multiply scattered photons
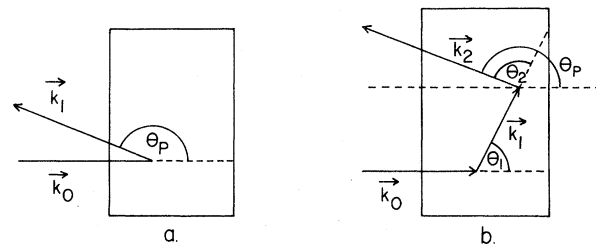

FIG. 1. Geometry for single and double Compton scattering. (a) A single scattering event, with $\vec{k}_0$ the initial photon direction, $\vec{k}_1$ the scattered photon direction, and $\theta_p = \cos^{-1}(\vec{k}_1 \cdot \vec{k}_2)$ the angle of scattering, which is also the angle of observation. (b) A double-scattering event. Here θ_p is still the angle of observation, but it is no longer equal to either of the actual scattering angles θ_1 or θ_2.

affect the observed wavelength or energy spectrum? Only the first question will be considered here; the second will be dealt with in paper II.

Recently, considerable attention has been given to the problem of multiple scattering, extending earlier analytic results[3] and utilizing Monte Carlo techniques[4,5] for numerical calculation of multiple scattering effects. The Monte Carlo method appears to be the only means for providing complete, quantitative answers to our questions above, and we have undertaken such a study. Here, however, we present a number of analytic results in an effort to derive a qualitative understanding of multiple scattering.

Several of the quantities calculated in this paper have been considered elsewhere, but generally in less detail and/or from very different points of view. Felsteiner and Pattison[6] and Williams and Halonen[7] have used Monte Carlo techniques to calculate total probabilities and spectral distributions of multiple scattering from a cylindrical sample, but have not dealt in detail with the angular distribution of multiply scattered radiation. Kirkpatrick[3b] and McIntire[8] have carried out analytic calculations of the double-scattered intensity and spectrum, but only at a single angle of observation (90° and 180°, respectively) in each case. Dumond[3a] considered the probability of multiple scattering as a function of angle, but for a somewhat unrealistic sample geometry, and with approximations very different from those of the present work.

Chandrasekhar[9] and O'Rourke[10] have obtained the total spectral distribution of Compton-scattered radiation via an approximate solution to the Boltzmann equation. However, in addition to making some rather drastic approximations, this approach is incapable of distinguishing the singly scattered from the multiply scattered contribution. It is therefore of little practical use to those interested in electronic momentum distributions. A technique based on the theory of Markov processes, suggested by Brockwell,[11] suffers from the same drawback, through it does yield angular distributions of total scattering over a discrete grid of solid angles.

Most other work[12,13] has dealt with the spectral distribution of doubly scattered radiation, and in paper II of this series we shall take up that problem. Paper III will utilize the results of Monte Carlo calculations to assess the accuracy of the approximations employed in our analytic work and to extend the qualitative insights derived there. Finally, in paper IV, we shall discuss how results like those obtained in our earlier papers may be used to improve the accuracy of electronic momentum distributions derived from experimental Compton profiles which contain unavoidable and often sizable contributions from multiple scattering.

II. BASIC PROCESSES AND VARIABLES

A. Fundamental equations

Three equations represent the basic physical processes taking place in a Compton-scattering experiment. These processes are:

(i) Exponential attentuation of the intensity of a photon beam on traversing a distance l:

$$I/I_0 = e^{-\mu l}, \tag{2}$$

where μ is the (total) attenuation coefficient of the scatterer.

(ii) The probability of scattering a photon into some direction Ω according to a differential cross section $d\sigma/d\Omega$,

$$\frac{d\sigma}{d\Omega} = f(\Omega, E_1, \vec{\epsilon}_1, E_2, \vec{\epsilon}_2), \tag{3}$$

where $d\Omega$ is an element of solid angle, and E_i and $\vec{\epsilon}_i$ represent the energy and polarization of the photon, with $i = 1$ for the incident and $i = 2$ for the scattered photon. We shall be considering several different forms for $d\sigma/d\Omega$, which for the moment we leave unspecified.

(iii) The change in energy of a scattered photon according to Eq. (1), which, written in terms of energy in electron rest mass units and atomic units becomes

$$\frac{1}{E_1} - \frac{1}{E_0} = 2\sin^2\tfrac{1}{2}\theta + \frac{2}{E_0}\frac{p_z}{137}\sin\tfrac{1}{2}\theta. \tag{4}$$

The intensity of multiple scattering is then a function of the many variables which appear explicitly or implicitly in the above equations. For example, the energies E_i of the photons appear explicitly in (3) and (4), but μ in Eq. (2) is also a function of photon energy. Sample geometry is critical in determining both the average and the range of values of l in Eq. (2).

In this analytic study of multiple scattering and in later Monte Carlo studies, we shall attempt to assess the relative importance of these variables.

B. Simple model

For the present analytic calculation, consider the following simple model for a Compton-scattering experiment. A cylindrical sample of radius R_f and thickness t is irradiated by a circular beam of radius R_b ($\leq R_f$) of unpolarized photons with a single incident energy E_0. The photons enter perpendicular to the cylinder face and are observed at angle θ_p (Fig. 2). It is assumed that the electrons within the sample are stationary.
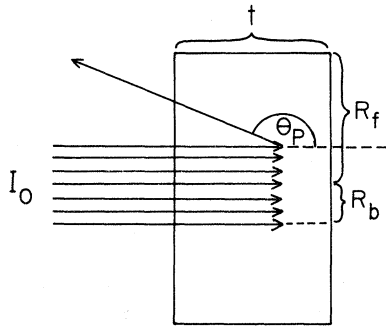
FIG. 2. Geometry for simple Compton-scattering experiment. θ_p is the angle at which scattered photons are observed. For 1-scattered photons, θ_p will also be the scattering angle.

The attenuation coefficient μ is the sum of the attentuation coefficients for all process occurring in the sample. In a typical Compton experiment these are photoelectric absorption, Rayleigh (elastic) scattering, and Compton (inelastic) scattering; μ is taken to be the same for incident and scattered photons. Only Compton events will be considered in detail. Elastic scattering and photoelectric absorption will be considered only in terms of their contribution to the attenuation coefficient μ.

For the differential cross section we employ the classical (Thomson) expression averaged over all polarizations:

$$\frac{d\sigma}{d\Omega} = \tfrac{1}{2}r_0^2(1 + \cos^2\theta),$$

where θ is the scattering angle and r_0 the classical electron radius. We shall use a cross section of this form, but normalized to unity and also denoted by $d\sigma/d\Omega$:

$$\frac{d\sigma}{d\Omega} = \frac{3}{16\pi}(\cos^2\theta + 1), \qquad (5)$$

with

$$\int d\Omega \frac{d\sigma}{d\Omega} = 1 .$$

Suppose that the probability of multiple scattering is a function of m variables. Let $\vec{V}$ be an ordered m-tuple of those variables. Define $P_n(\vec{V})$ as the total probability of a photon's scattering exactly n times within the cylinder, and then escaping. Define also the angular distribution of the n-scattered photons $(\partial P_n/\partial \Omega_p)d\Omega_p$ as the probability of observing an n-scattered photon within $d\Omega_p$ of solid angle at Ω_p. Only P_1, $\partial P_1/\partial \Omega_p$, and $\partial P_2/\partial \Omega_p$ for restricted cases will be explicitly calculated.

III. SOME IMMEDIATE DEDUCTIONS

From Eq. (2) and the experimental geometry described above, the probability of a photon's passing through the sample without scattering is $e^{-\mu t}$, and hence the probablity of scattering at least once is $1 - e^{-\mu t}$. Therefore,

$$\sum_{n=1}^{\infty} P_n(\vec{V}) = 1 - e^{-\mu t}, \qquad (6)$$

and it follows that

$$P_1(\vec{V}) \leqslant 1 - e^{-\mu t}. \qquad (7)$$

A lower bound for $P_1(\vec{V})$ will be derived later.

Figure 3(a) shows $d\sigma/d\Omega$ as in Eq. (5). This is the angular distribution $\partial P_1/\partial \Omega$ of one-scattered photons for a sample consisting of a single stationary electron. The angular distribution of photons scattered first by a single electron and then again by a spherical shell of electrons centered on the first electron is

$$\frac{\partial P_2}{\partial \Omega_p} = \int d\Omega_1 \frac{3}{16\pi}(\cos^2\theta_1 + 1)\frac{3}{16\pi}(\cos^2\theta_2 + 1),$$
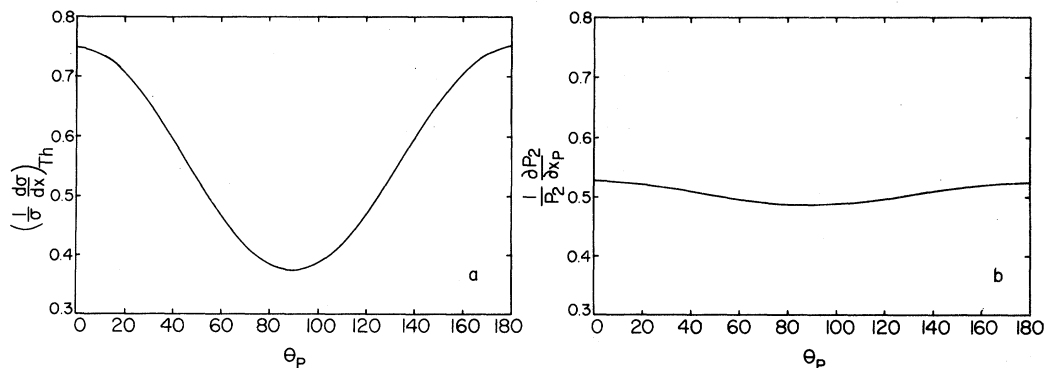
where[3,14]

FIG. 3. Normalized Thomson differential-scattering cross sections as a function of angle of observation.   (a) Single scattering from a single stationary electron. (b) Double scattering, Eq. (9) (see text).

$$\cos\theta_2 = \sin\theta_p \sin\theta_1 \cos(\varphi_p - \varphi_1) + \cos\theta_p \cos\theta_1 . \quad (8)$$

On carrying out the integral, we find that

$$\frac{\partial P_2}{\partial\Omega_p} = \frac{3}{160\pi}(13 + \cos^2\theta_p) . \quad (9)$$

This function is shown in Fig. 3(b). Both Eq. (9) and Fig. 3 clearly show that the angular distribution of two-scattered photons in this simple case is nearly isotropic. Since the initial angular distribution $\partial P_0/\partial\Omega_p$ was a δ function at $\theta = 0$, $\partial P_0/\partial\Omega_p = (1/2\pi)\delta(0)$, it is obvious that the scattering process "randomizes" the angular distribution quite rapidly, from δ function to essentially isotropic in only two scatterings. Further, it is easy to show[14] that an isotropic distribution remains so on undergoing a classical scattering as in (5).

We conclude that any anisotropies in the distributions $\partial P_n/\partial\Omega_p$ observed for a finitely large sample result primarily from the sample geometry and not from the differential-scattering law. Thus an approximate calculation to assess the effect of geometry on multiple scattering might be able to utilize an isotropic differential scattering cross section[15] $d\sigma/d\Omega = 1/4\pi$.

IV. SINGLE SCATTERING

A. Coordinate systems

Let us construct a Cartesian coordinate system with the z axis along the cylinder axis. One face of the cylinder is at $z = 0$, the other at $z = t$. The origin is at the center of the first face [Fig. 4(a)].

A cylindrical system of coordinates can be constructed with the same z axis and origin as above, and with r the distance from the z axis and γ the
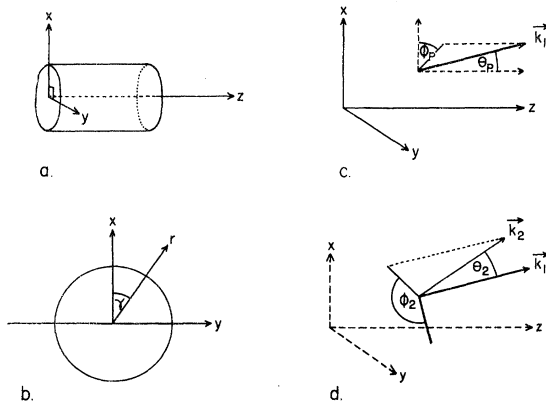
angle with the x axis [Fig. 4(b)].

A primary (or observation) system S_p of spherical coordinates (θ_p, φ_p) may also be defined such that $\theta_p = 0$ is parallel to the z axis and φ_p is measured from the x axis [Fig. 4(c)].

Direction vectors $\vec{k}$ are defined as unit vectors in S_p with angles (θ_p, φ_p). In general, a photon enters the cylinder face at $(r, \gamma, 0)$ with direction vector $\vec{k}_0 = (0, 0)$, and can scatter within the cylindrical sample at (r, γ, z) into a new direction $\vec{k}_1$ defined by $(\theta_1, \varphi_1) = (\theta_p, \varphi_p)$ in S_p. Another spherical system S_1 is now constructed by rotating the polar (θ) axis into the direction $\vec{k}_1$. The old azimuthal (φ) axis is rotated so that it now intersects the cylinder axis [Fig. 4(d)]. If the photon scatters again before escaping, the new direction is specified in S_1 by (θ_2, φ_2). The extension to n scattering is similar.

B. Total scattering probability

We define a *differential probability* $d\mathcal{P}_1$ as the probability that a photon enters the sample within an $r\,dr$ neighborhood of r and a $d\gamma$ neighborhood of γ, Compton scatters within a dz neighborhood of z into a $\sin\theta\,d\theta$ neighborhood of θ_1 and a $d\varphi$ neighborhood of φ_1, and then escapes the cylinder by traversing a distance l from (r, γ, z) along the direction (θ_1, φ_1) to the cylinder boundary. The distance l is a function of θ_1, φ_1, R_f, z, and t. $d\mathcal{P}_1$ is given by the product of the normalized probability densities of the above events multiplied by their respective differentials:

$$d\mathcal{P}_1 = \frac{2r}{R_b^2} dr \frac{d\gamma}{2\pi} (\mu e^{-\mu z} dz) \frac{d\sigma}{d\Omega} d\Omega \, f_C e^{-\mu l}, \quad (10\text{a})$$

where f_C is the probability that a photon-electron scattering event will be a Compton event. Then

$$f_C = \frac{\sigma_C}{\sum_i \sigma_i} = \frac{\mu_C}{\sum_i \mu_i},$$

where the σ_i's and μ_i's are the respective cross sections and attenuation coefficients for the possible photon-electron processes: Compton scattering, elastic scattering, photoelectric absorption, and pair production, this last being negligible under normal experimental conditions.

A *cumulative probability distribution* $\mathcal{P}_1(R, \Gamma, t, \mu, \theta_1, \varphi_1, R_f)$ is now defined as the probability that a photon enters the sample at $(r, \gamma, 0)$ with

$$0 < r \leqslant R \leqslant R_b, \text{ and } 0 < \gamma \leqslant \Gamma \leqslant 2\pi,$$

then scatters at (r, γ, z) into (θ_1', φ_1') with

$$0 < z \leqslant t,$$

$$0 < \theta_1' \leqslant \theta_1 \leqslant \pi,$$

$$0 < \varphi_1' \leqslant \varphi_1 \leqslant 2\pi,$$

FIG. 4. Coordinate systems: (a) Cartesian system; (b) Cylindrical system; (c) Primary spherical system S_p, and first scattering direction $\vec{k}_1$ with $\theta_1 = \theta_p$, $\varphi_1 = \varphi_p$; (d) Spherical system S_1 and second scattering direction $\vec{k}_2 = (\theta_2, \varphi_2)$ relative to $\vec{k}_1$.

and finally escapes the cylinder:

$$\mathcal{P}_1(R, \Gamma, t, \mu, \theta_1, \varphi_1, R_f) = f_C \int_0^R dr \frac{2r}{R_b^2} \int_0^\Gamma d\gamma \frac{1}{2\pi} \int_0^t dz\, \mu e^{-\mu z} \int_0^{\theta_1} d\theta_1' \sin\theta_1' \int_0^\varphi d\varphi_1' \frac{d\sigma}{d\Omega'} e^{-\mu l}. \tag{10b}$$

For the moment, we set $f_C = 1$.

On taking $R = R_b$, $\Gamma = 2\pi$, $\theta_1 = \pi$, $\varphi_1 = 2\pi$, we obtain the *total* probability of 1-scattering, $P_1(\vec{V})$:

$$P_1(R_b, t, \mu, R_f) = \mathcal{P}_1(R_b, 2\pi, t, \mu, \pi, 2\pi, R_f). \tag{10c}$$

The integrals required to calculate P_1 are difficult. If, however, we take $t \ll R_f - R_b$, then a closed expression for $P_1(R_b, t, \mu, R_f)$ can be found in terms of higher transcendental functions.[14] With the above restriction, P_1 becomes independent of R_b and R_f, and in fact depends only upon the "optical thickness" $\mu t \equiv \omega$. We denote the total probability of single scattering in this "infinite-radius" limit by $P_1^\infty(\omega)$.

An interesting conclusion follows from a comparison of scattering from this limiting geometry with that from a finite radius cylinder. Figure 5(a) depicts a number of single-scattering events for a cylinder with finite R_f and optical thickness ω. The paths labeled f lead to escape through the faces, while those labeled s result in escape through the sides. Imagine now that R_f is increased while ω is held constant. The sum of probabilities for all multiplicities of scattering is independent of R_f [Eq. (6)]. Figure 5(a) shows that f events of single scattering are unaffected by an increase in R_f, but that the probability of s events decreases. Then it must be true that a lower limit of single scattering is obtained as $R_f \to \infty$, so that

$$P_1^\infty(\omega) \leq P_1(\mu, t, R_f, R_b) \leq 1 - e^{-\omega}. \tag{11}$$

Figure 6 shows the dependence of total P_1^∞ on ω as well as the variation of the forward- $(\theta_1 < 90°)$ and back- $(\theta_1 > 90°)$ scattered components. Note that the back-scattered portion monotonically increases to an asymptotic value of 0.16764, and

that the forward portion rises to a maximum and then decreases asymptotically to zero. Figure 5(b) depicts several scattering events for a cylinder of infinite radius and optical thickness ω_1. Forward-scattered photons are denoted by f and back-scattered photons by b. A photon need not scatter at all, as indicated by path III. Consider now an increase in optical thickness to $\omega = \omega_1 + \Delta\omega$. The back-scattered events remain unaltered (paths I and IV). There is, however, an increased probability that the f photon (path II) will be scattered again. Also, there is increased probability that the photon formerly transmitted (path III) will now be scattered either forward or backward. Thus, forward single scattering may be expected to increase to a maximum with increasing ω because of an increase in events as in path III, and then decrease to zero because of the increased probability that any forward-scattered photons will be scattered again as in path II.

In an actual experiment, only those photons are observed which scatter into θ_p in some small range of angles. We now turn to a consideration of the angular distribution $\partial P_1^\infty(\omega, \theta)/\partial\theta$, or, letting $x = \cos\theta$, $\partial P_1^\infty(\omega, x)/\partial x$.

C. Angular distributions

From Eq. (10) and the definition of $P_1^\infty(\omega)$, we may write[16]

$$P_1^\infty(\omega, \theta_1) = \int_0^t dz\, \mu e^{-\mu z} \int_0^{\theta_1} d\theta' \sin\theta'$$

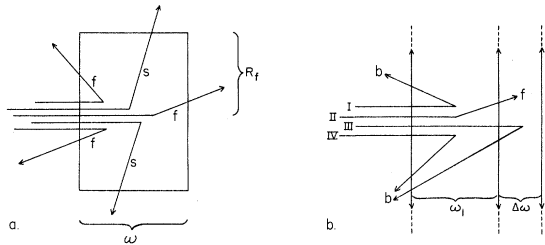$$\times \int_0^{2\pi} d\varphi' \frac{d\sigma}{d\Omega'} e^{-\mu l}, \tag{12}$$

FIG. 5. Paths for some single-scattering events. (a) Finite-radius cylinder showing photons escaping through faces (f) and sides (s). (b) Infinite-radius case and effects of increasing optical thickness on forward- (f) and back- (b) scattered photons.
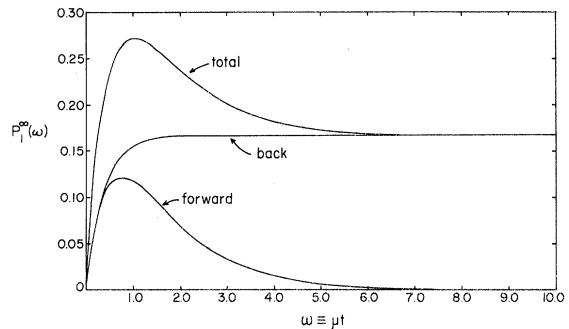

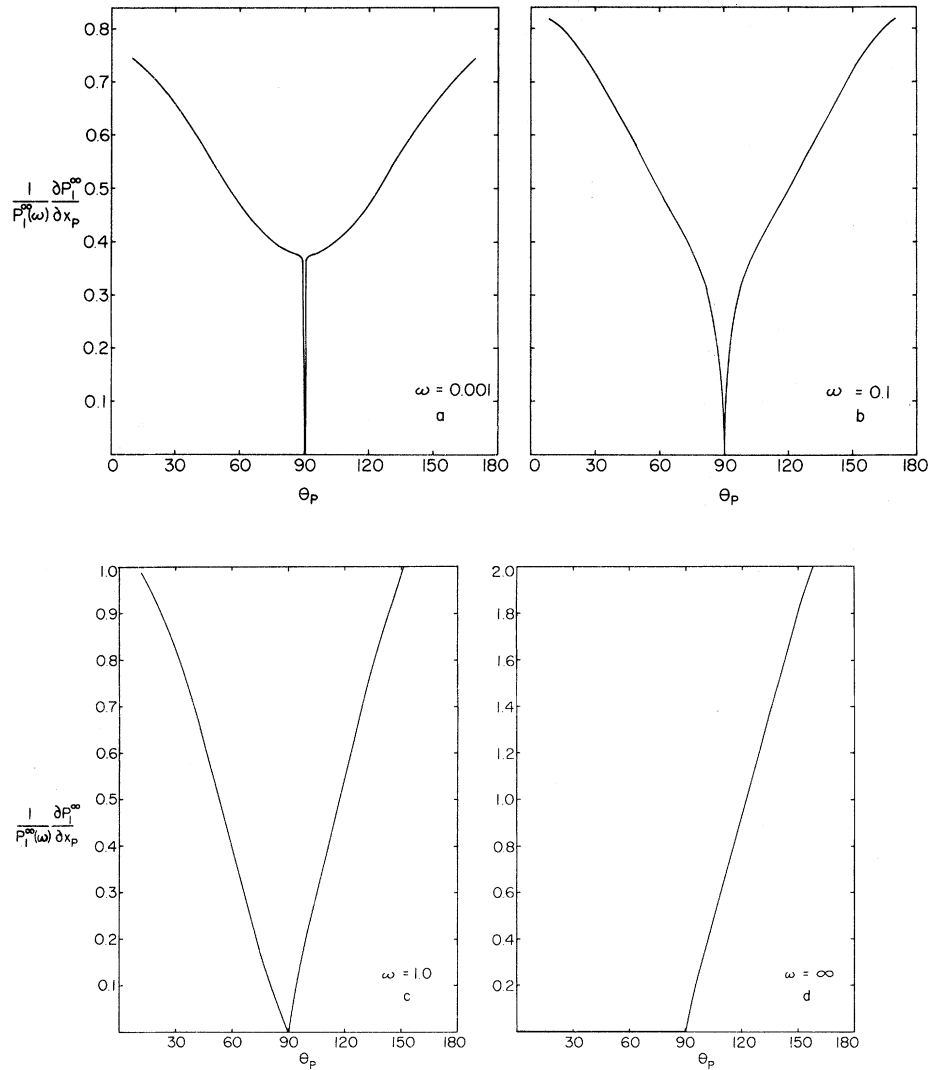FIG. 6. Probability $P_1^\infty(\omega)$ of single scattering for cylindrical sample with $R_f = \infty$.

FIG. 7. Normalized angular distribution for single scattering from cylindrical samples with varying thickness and $R_f = \infty$. (a) $\omega = 0.001$; (b) $\omega = 0.1$; (c) $\omega = 1.0$; (d) $\omega = \infty$.

where, for single scattering, $\theta_1 = \theta_p$, the angle of observation. The angular distribution for single scattering may then be found by differentiating Eq. (12) with respect to θ_1 or by changing variable to $x = \cos\theta_1$ and taking $\partial/\partial x$ of $P_1^\infty(\omega, x)$.[16] The result is given explicitly in Ref. 14.

Figure 7 displays a number of these distributions for optical thicknesses ω ranging from 0.001 to ∞. These angular distributions have been normalized to 1, so that their shapes for different ω may easily be compared with one another. At very small ω, $\partial P_1^\infty/\partial x$ is nearly identical with the single-electron Thomson cross section [Fig. 3(a)], except, of course, for the immediate neighborhood of $\theta = \frac{1}{2}\pi$, which is forbidden by the infinite-radius geometry. As ω increases, an asymmetry about $\theta = \frac{1}{2}\pi$ is introduced; i.e., for $x > 0$, we have

$$\frac{\partial P_1^\infty(\omega, -x)}{\partial x} > \frac{\partial P_1^\infty(\omega, x)}{\partial x},$$

whereas equality holds for the single-electron expression. From our earlier remarks on Thomson and isotropic scattering and on forward-vs-back scattering, we conclude that this symmetry is the result of sample geometry (and of the exponential attenuation).

In Tables I and II we compare the total probability of single scattering and the angular distributions $\partial P_1^\infty(\omega, x)/\partial x$, respectively, for isotropic (iso) and Thomson (Th) scattering. The total probabilities never differ by more than 10%, but the angular distributions agree much less well. For small ω, the isotropic distribution (except around 90° or $x = 0$) is, of course, a constant, in contrast

TABLE I. Total probability of single scattering from Thomson and isotropic cross sections as function of optical thickness ω.

ω	$P_1(\omega)$ (Thomson)	$P_1(\omega)$ (isotropic)	Fractional difference
0.001	0.9964×10^{-3}	0.9955×10^{-3}	-0.0009
0.01	0.9725×10^{-2}	0.9675×10^{-2}	-0.0051
0.10	0.8186×10^{-1}	0.7966×10^{-1}	-0.0269
0.20	0.1399	0.1342	-0.0407
0.30	0.1821	0.1728	-0.0511
0.40	0.2127	0.2001	-0.0592
0.50	0.2347	0.2192	-0.0660
1.00	0.2715	0.2482	-0.0858
2.00	0.2369	0.2138	-0.0975
3.00	0.2012	0.1820	-0.0954
4.00	0.1823	0.1657	-0.0911
5.00	0.1738	0.1585	-0.0880
10.00	0.1677	0.1535	-0.0847

to the Thomson distribution which is greater at 0° and 180° than at 90°. For $\omega = 1.0$, the effects of geometry begin to be felt, though there is still significant difference between the Thomson and isotropic cases. As ω continues to grow, the relative difference between the two cases decreases to a nonzero limit.

An isotropic cross section will scatter relatively more photons into the region around $\theta = 90°$ than will the Thomson cross section. In this region, the path length through the sample is large (since $R_f = \infty$), and thus it is quite likely that photons will

multiply rather than singly scatter in this region. Therefore, it is to be expected that

$$[P_1^\infty(\omega)]_{\text{iso}} < [P_1^\infty(\omega)]_{\text{Th}} \qquad (13)$$

and

$$\left(\frac{\partial P_1^\infty(\omega, x)}{\partial x}\right)_{\text{iso}} < \left(\frac{\partial P_1^\infty(\omega, x)}{\partial x}\right)_{\text{Th}} \qquad (14a)$$

for angles near 0° and 180°, while

$$\left(\frac{\partial P_1^\infty(\omega)}{\partial x}\right)_{\text{iso}} > \left(\frac{\partial P_1^\infty(\omega, x)}{\partial x}\right)_{\text{Th}} \qquad (14b)$$

for angles near 90°. Tables I and II bear out this expectation.

With certain restrictions on the sample geometry and scattering angle, the angular distributions calculated here will apply to finite cylinders as well. The requirement is that the observed singly scattered photons escape only through the cylinder faces. For a finite sample of thickness t and radius R_f, and a beam of radius R_b, this condition requires a scattering angle θ such that

$$|\cos\theta| > t/[(R_f - R_b)^2 + t^2]^{1/2}$$

or

$$R_f - R_b > t |\tan\theta|. \qquad (15)$$

Equation (15) may be derived from the geometric relations given in the Appendix. For a typical experimental arrangement with $\theta = 150°$ and t and R_b on the order of 0.1 to 2 cm, condition (15) will be

TABLE II. Angular distributions for single scattering from Thomson and isotropic cross sections.

$\cos\theta_p$	$\omega = 0.1$ $(\partial P_1/\partial x)_{\text{Th}}$	$(\partial P_1/\partial x)_{\text{iso}}$	$\omega = 1.0$ $(\partial P_1/\partial x)_{\text{Th}}$	$(\partial P_1/\partial x)_{\text{iso}}$	$\omega = 5.0$ $(\partial P_1/\partial x)_{\text{Th}}$	$(\partial P_1/\partial x)_{\text{iso}}$
-0.975	0.0405	0.0284	0.3135	0.2143	0.3611	0.2468
-0.875	0.0364	0.0283	0.2727	0.2060	0.3090	0.2333
-0.775	0.0328	0.0281	0.2355	0.1962	0.2621	0.2183
-0.675	0.0295	0.0278	0.2016	0.1846	0.2200	0.2015
-0.575	0.0267	0.0275	0.1704	0.1707	0.1822	0.1825
-0.475	0.0241	0.0270	0.1414	0.1538	0.1480	0.1610
-0.375	0.0219	0.0263	0.1137	0.1329	0.1167	0.1364
-0.275	0.0197	0.0251	0.0862	0.1068	0.0870	0.1078
-0.175	0.0172	0.0229	0.0575	0.0744	0.0576	0.0745
-0.075	0.0122	0.0167	0.0263	0.0349	0.0263	0.0349
$+0.075$	0.0120	0.0163	0.0113	0.0149	0.0002	0.0003
$+0.175$	0.0170	0.0226	0.0299	0.0387	0.0006	0.0007
$+0.275$	0.0196	0.0250	0.0523	0.0648	0.0010	0.0013
$+0.375$	0.0218	0.0262	0.0766	0.0895	0.0017	0.0020
$+0.475$	0.0241	0.0269	0.1023	0.1113	0.0028	0.0030
$+0.575$	0.0266	0.0274	0.1298	0.1300	0.0044	0.0044
$+0.675$	0.0295	0.0277	0.1594	0.1460	0.0070	0.0064
$+0.775$	0.0327	0.0280	0.1917	0.1597	0.0107	0.0089
$+0.875$	0.0363	0.0282	0.2270	0.1714	0.0159	0.0120
$+0.975$	0.0404	0.0284	0.2657	0.1816	0.0231	0.0158

easily satisfied, and it probably holds for many of the experiments which are currently being performed.

V. DOUBLE SCATTERING

A. Total scattering probability

As in the case of single scattering, we define a differential probability $d\mathcal{P}_2$ as the probability that a photon enters the sample within an $r\,dr$ neighborhood of r and a $d\gamma$ neighborhood of γ, then Compton scatters within a dz neighborhood of z into a $\sin\theta\,d\theta$ neighborhood of θ_1 and a $d\varphi$ neighborhood of φ_1, Compton scatters again in a dl'_2

neighborhood of l'_2 into a $\sin\theta_2\,d\theta_2$ neighborhood of θ_2 and a $d\varphi_2$ neighborhood of φ_2, and finally escapes the cylinder by traveling a distance l_3 to the cylinder boundary. The distance l'_2 from the first scattering point to the second is less than or equal to the distance l_2 from the first scattering point to the cylinder boundary. As above, l_2 is a function of z, θ_1, φ_1, R_f, and t (see Appendix). The angles θ_2 and φ_2 (the final direction of the photon) are defined in the coordinate system S_1 [Fig. 4(d)], which has $\tilde{k}_1$ as the polar axis. The distance l_3 from the second scattering to the cylinder boundary depends upon z, θ_1, φ_1, R_f, t, l'_2, θ_2, and φ_2.

Proceeding as before, we obtain a cumulative probability distribution

$\mathcal{P}_2(R, \Gamma, t, \mu, \theta_1, \varphi_1, \theta_2, \varphi_2, R_f)$

$$= f_C^2 \int_0^R dr \frac{2r}{R_b^2} \int_0^\Gamma \frac{1}{2\pi} \int_0^t dz\,\mu\,e^{-\mu z} \int_0^{\varphi_1} d\varphi'_1 \int_0^{\theta_1} d\theta'_1 \sin\theta'_1 \frac{d\sigma}{d\Omega_1}\, \int_0^{l_2} dl_2\,\mu\,e^{-\mu l'_2} \int_0^{\varphi_2} d\varphi'_2 \int_0^{\theta_2} d\theta'_2 \sin\theta'_2 \frac{d\sigma}{d\Omega'_2} e^{-\mu l_3}, \tag{16}$$

with f_C defined as before. The R_f dependence is contained implicitly in l_2 and l_3.

On setting $R = R_b$, $\Gamma = \varphi_1 = \varphi_2 = 2\pi$, and $\theta_1 = \theta_2 = \pi$, we obtain the total probability of double scattering, $P_2(\vec{V}) = P_2(R_b, t, \mu, R_f)$. In the special case $\omega \ll \mu$ $(R_f - R_b)$, we find

$$P_2^\infty(\omega) = \int_0^t dz\,\mu\,e^{-\mu z} \int_0^{2\pi} d\varphi_1 \int_0^\pi d\theta_1 \sin\theta_1 \frac{d\sigma}{d\Omega_1} \int_0^{l_2} dl'_2\,\mu\,e^{-\mu l'_2} \int_0^{2\pi} d\varphi_2 \int_0^\pi d\theta_2 \sin\theta_2 \frac{d\sigma}{d\Omega_2} e^{-\mu l_3},$$

with

$$\frac{d\sigma}{d\Omega_j} = \frac{3}{16\pi}(\cos^2\theta_j + 1). \tag{17}$$

A change of variable from Ω_2 to Ω_p, the observation of primary system, is made. Since this is merely a rotation, the Jacobian is unity, and we simply replace the volume element $d\varphi_2 d\theta_2 \sin\theta_2$ by $d\varphi_p d\theta_p \sin\theta_p$. Another change of variables, from θ_i to $x_i = \cos\theta_i$, $i = 1, p$, is made, so that

$$P_2^\infty(\omega) = \int_0^t dz\,\mu\,e^{-\mu z} \int_0^{2\pi} d\varphi_1 \int_{-1}^1 dx_1 \frac{3}{16\pi}(x_1^2 + 1) \int_0^{l_2} dl'_2\,\mu\,e^{-\mu l'_2} \int_0^{2\pi} d\varphi_p \int_{-1}^1 dx_p \frac{3}{16\pi}(\cos^2\theta_2 + 1)e^{-\mu l_3}. \tag{18}$$

If we now replace 1 by x_p as the upper limit in the last integral and differentiate with respect to x_p, we obtain the angular distribution $\partial P_2^\infty(\omega, x_p)/\partial x_p$. This quantity is calculated in closed form in terms of higher transcendental functions in Ref. 14. The total probability of double scattering, $P_2^\infty(\omega)$, is not calculated directly, but is obtained by numerically integrating this angular distribution.

Unfortunately, $P_2^\infty(\omega)$ is *not* a lower bound for $P_2(\vec{V})$. It is not true, as it was for single scattering, that increasing R_f from some finite value causes $P_2(\vec{V})$ to decrease monotonically. Although the probability of double scattering through the sides does strictly decrease, the total $P_2(\vec{V})$ can actually increase at the expense of $P_1(\vec{V})$. We do

have

$$0 \le P_2(\vec{V}) \le 1 - e^{-\omega} - P_1^\infty(\omega) \le 1 - e^{-\omega} - P_1(\vec{V}). \tag{19}$$

Figure 8 shows that the behavior of $P_2^\infty(\omega)$ for $0 < \omega \le 10.0$ is qualitatively similar to that of $P_1^\infty(\omega)$ (Fig. 6) and to the Monte Carlo results of Felsteiner and Pattison.[6] $P_2^\infty(\omega)$ is always less than $P_1^\infty(\omega)$, but peaks at $\omega \sim 1.6$ compared with $\omega \sim 1.0$ for $P_1^\infty(\omega)$. For large ω, $P_2^\infty(\omega) = 0.092\,83$, while $P_1^\infty(\omega) = 0.167\,64$.[17]

B. Angular distributions

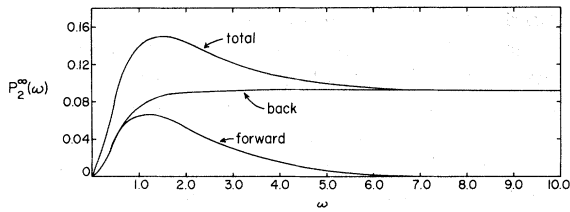It has already been noted that the angular distribution of doubly scattered photons for an elec-

FIG. 8. Probability $P_2^\infty(\omega)$ of double scattering for cylindrical sample with $R_f = \infty$.

tron surrounded by a spherical shell of electrons is nearly isotropic. For small ω, $\partial P_1(\omega,x)/\partial x_p$ is quite similar to the single-electron angular distribution except in the immediate neighborhood of $x_p = 0$. Figure 9, however, shows that the angular distribution of double scattering for very thin cylindrical samples of infinite radius is quite different from that shown in Fig. 3(b). For such samples, $\partial P_2^\infty/\partial x_p$ actually increases as $|x_p|$ decreases

from 1, then falls rapidly to zero at $x_p = 0$. The rapid decrease near $x_p = 0$ results from the infinite-radius condition. To understand the appearance of the maximum in $\partial P_2/\partial x_p$, we note that the small value of ω makes it unlikely for a photon to two-scatter at all, but if it does two-scatter, it is most likely to do so around $x_p = 0$, where the path length through the sample is large. As ω increases, 2-scattering increases around $x = \pm 1$, and becomes less likely around $x = 0$, where higher-order scattering dominates, so the maximum disappears [Fig. 9(c)]. We note also that, like $\partial P_1^\infty/\partial x_p$, $\partial P_2^\infty/\partial x_p$ displays an asymmetry about $x_p = 0$ which increases with increasing ω.

To study double scattering for an isotropic differential cross section, we simply replace Eq. (17) by

$$d\sigma/d\Omega_j = 1/4\pi$$

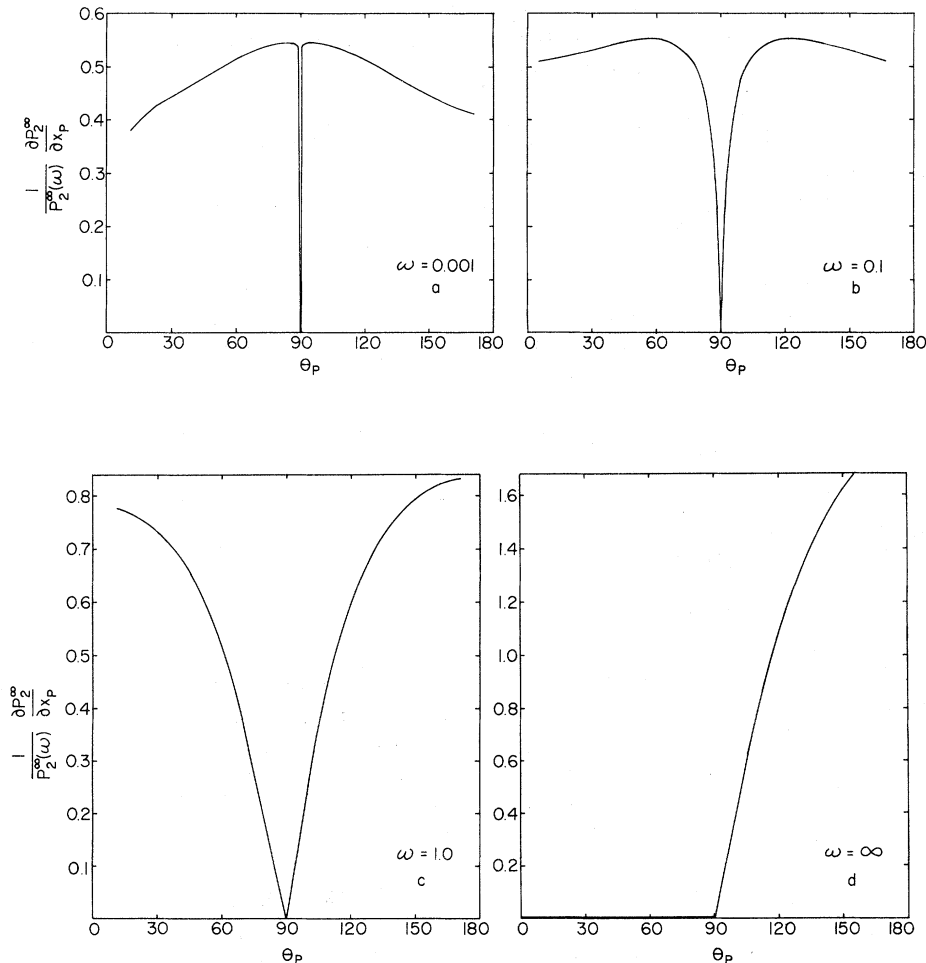and proceed as in Eq. (16) and Ref. 14. We obtain

FIG. 9. Normalized angular distributions for double scattering from cylindrical samples with varying thicknesses and $R_f = \infty$. (a) $\omega = 0.001$; (b) $\omega = 0.1$; (c) $\omega = 1.0$; (d) $\omega = \infty$.

TABLE III. Total probability of double scattering from Thomson and isotropic cross sections as a function of optical thickness ω.

ω	$P_2(\omega)$ (Thomson)	$P_2(\omega)$ (isotropic)	Fractional differences
0.001	0.3107×10^{-5}	0.3856×10^{-5}	0.2411
0.01	0.2192×10^{-3}	0.2686×10^{-3}	0.2254
0.10	0.011 06	0.012 97	0.1727
0.20	0.030 33	0.034 78	0.1467
0.30	0.050 85	0.057 42	0.1292
0.40	0.070 17	0.078 28	0.1156
0.50	0.087 34	0.096 44	0.1042
1.00	0.1382	0.1475	0.0673
2.00	0.1437	0.1489	0.0362
3.00	0.1228	0.1265	0.0301
4.00	0.1077	0.1114	0.0344
5.00	0.099 62	0.1036	0.0400
10.00	0.092 43	0.0968	0.0473

$$\left(\frac{\partial P_2^\infty}{\partial x_p}\right)_{\text{iso}} = \begin{cases} \frac{1}{4}G_0(\omega, x_p, 1), & -1 \le x_p < 0 \\ \frac{1}{4}e^{-\omega/x_p}G_0(\omega, x_p, 1), & 0 < x_p \le 1 \\ 0, & x_p = 0. \end{cases}$$

The function G_0 is defined and evaluated in Ref. 14.

The total probabilities and angular distributions of double scattering using the Thomson and isotropic cross sections are presented in Tables III and IV. We find that the inequalities (13) and (14a) obtained for single scattering are now reversed,

though the reason is the same: the isotropic cross-section scatters more photons into the central region where the path length through the sample is large and multiple scattering is more likely.

VI. LIMITATIONS AND RESTRICTIONS

The above calculations have been based upon a rather idealized view of a Compton-scattering experiment. Since the aim of this analytic work was to provide some qualitative insight into the problem of multiple scattering, we have not attempted to treat a more realistic model analytically. From even the present simplified model, it is evident that the calculations involved would be formidable, if not impossible. In paper III of this series we shall show that Monte Carlo techniques provide a much more attractive route to accurate results for more detailed models, but that the simple models treated here are not as unrealistic at one might think. Nevertheless, in this section we shall take explicit note of some of the restrictions of the present treatment, and indicate how they might be dealt with, at least in approximate fashion.

A. Finite geometry

Our calculations have been greatly facilitated by the choice of $R_f = \infty$. For a general, finite set of cylinder dimensions, the integrals to be done seem so complicated as to make an exact treatment hopeless. However, at least in certain cases, such a

TABLE IV. Angular distribution from Thomson and isotropic cross sections.

$\cos\theta$	$\omega = 0.1$		$\omega = 1.0$	
	$(\partial P_2/\partial x)_{\text{Th}}$	$(\partial P_2/\partial x)_{\text{iso}}$	$(\partial P_2/\partial x)_{\text{Th}}$	$(\partial P_2/\partial x)_{\text{iso}}$
-0.975	0.005 70	0.007 37	0.1144	0.1244
-0.875	0.005 85	0.007 33	0.1099	0.1189
-0.775	0.005 97	0.007 27	0.1045	0.1126
-0.675	0.006 06	0.007 21	0.0978	0.1050
-0.575	0.006 11	0.007 12	0.0897	0.0960
-0.475	0.006 10	0.006 99	0.0797	0.0851
-0.375	0.006 02	0.006 81	0.0674	0.0718
-0.275	0.005 81	0.006 50	0.0522	0.0556
-0.175	0.005 32	0.005 91	0.0341	0.0362
-0.075	0.003 86	0.004 28	0.0140	0.0149
$+0.075$	0.003 85	0.004 26	0.0095	0.0099
0.175	0.005 31	0.005 89	0.0251	0.0263
0.275	0.005 80	0.006 47	0.0415	0.0436
0.375	0.006 02	0.006 80	0.0563	0.0593
0.475	0.006 10	0.006 99	0.0690	0.0728
0.575	0.006 11	0.007 11	0.0796	0.0842
0.675	0.006 06	0.007 20	0.0884	0.0938
0.775	0.005 97	0.007 27	0.0958	0.1019
0.875	0.005 85	0.007 32	0.1019	0.1089
0.975	0.005 69	0.007 37	0.1071	0.1149

calculation may not be necessary.

We recall that for certain scattering angles and for t and R_b sufficiently smaller than R_f [Eq. (15)] our expressions for single scattering also hold for finite samples. While no such simple geometric constraint will make our double-scattering results exact for finite samples, it seems clear that satisfaction of the constraint of Eq. (15) or of a somewhat more stringent but by no means unattainable one should make it possible to restrict double scattering almost completely to the regions considered in our model. Also, standard experimental practice[5] involves the use of a sample holder which makes the walls of the cylinder essentially perfect absorbers. While this is not precisely equivalent to an infinite value of μR_f, it should bring scattering from the finite radius cylinder somewhat closer to our model.

Our results show that both total scattering and angular distributions for all orders of scattering approach asymptotic limits with increasing ω. Values of these quantities for ω values as small as 2.0 are quite close to their infinite-thickness limits. This indicates that for reasonably thin samples and narrow beams, even a sample radius of a few mean free paths might make the present treatment applicable. Preliminary Monte Carlo results support this conclusion, e.g., for copper samples of radius 1.0 cm in a beam of radius 0.5 cm at either x-ray ($E_0 \sim 15$ keV) or γ-ray ($E_0 \sim 60$ keV) energies.

Finally, for samples with $\omega \ll 1$, but R_f and R_b finite, it may be possible to carry out the resulting integrals for $P_1(\vec{V})$ and $P_2(\vec{V})$ approximately in terms of elliptic functions.

B. Other processes

Initially we set f_C, the fraction of events which are Compton events, equal to 1. To account for photoelectric absorption, elastic scattering, and pair production, we must obtain the cross sections for these processes for the sample of interest.[18] For single scattering, the total probability of observing a photon is the sum of the probabilities of observing a Compton-scattered photon and of observing an elastically scattered photon:

$$P_1(\vec{V}) = f_C P_1(\vec{V})_C + f_R P_1(\vec{V})_R . \tag{20a}$$

For double scattering,

$$P_2(\vec{V}) = f_C^2 P_2(\vec{V})_{CC} + f_C f_R P_2(\vec{V})_{CR}$$
$$+ f_R f_C P_2(\vec{V})_{RC} + f_R^2 P_2(\vec{V})_{RR}, \tag{20b}$$

where the subscripts denote the order and type of scattering, R for elastic (or Rayleigh) and C for Compton. The corresponding formulas for angular distributions are obtained by substituting

$\partial P_i(\vec{V}, x)/\partial x$ for $P_i(\vec{V})$, $i = 1, 2$, in Eq. (20).

The probabilities for elastic scattering are easily obtained from our results, since $(d\sigma/d\Omega)_R$ is equal to $(d\sigma/d\Omega)_C$ except at small angles (coherent scattering)[19]:

$$\left(\frac{d\sigma}{d\overline{\Omega}}\right)_R = \begin{cases} (x^2 + 1)/N_R, & -1 \le x \le x_1 \\ Z(x^2 + 1)/N_R, & x_1 < x \le 1, \end{cases} \tag{21}$$

where Z is the atomic number of the scattering material and x_1 is the cosine of the critical angle θ_C, given by

$$\theta_C \simeq Z^{1/3}/E_0(\text{keV}),$$

and

$$N_R = 2\pi[(Z + 1) + (\tfrac{1}{3}x_1^3 + x_1)(1 - Z)].$$

The special functions used to calculate the Compton-scattering probabilities and angular distributions have x_1 as a variable, so that the quantities in Eq. (21) can easily be evaluated. Williams $et\ al.$[12] have studied the effect of elastic scattering on spectral distributions in an extension of Dumond's earlier work[3a] on multiple scattering.

C. Differential scattering laws

Thus far, we have taken the differential scattering cross section $d\sigma/d\Omega$ to be the Thomson (classical) cross section for unpolarized photons [Eq. (5)]. The corresponding cross section for polarized photons is[19]

$$\frac{d\sigma}{d\Omega} = \frac{3}{8\pi}[1 - \sin^2\theta_1 \cos^2(\varphi_1 - \psi_0)], \tag{22}$$

where θ_1 and φ_1 are as before and ψ_0 is the angle between the initial polarization vector and the x axis.

It is easily shown, by interchanging the order of averaging over initial polarization and performing the integrals in Eq. (10b), that use of Eq. (22) in place of Eq. (5) does not change our single-scattering results. However, the polarization ψ_1 of the scattered photon now depends on the initial polarization ψ_0.[19] Thus, for double scattering the integration over ψ_0 is not simple, and use of Eq. (22) will not $a\ priori$ lead to the result obtained with Eq. (5). Recall, however, that similar results were obtained with Thomson and isotropic cross sections, indicating that these results are rather insensitive to the form of $d\sigma/d\Omega$, at least for moderately thick samples. The Monte Carlo calculations of paper III will provide a qualitative estimate of the effect of neglecting polarization.

Another choice for $d\sigma/d\Omega$ is the relativistic or Klein-Nishina (KN) cross section, which for polarized photons is

$$\left(\frac{d\sigma}{d\Omega}\right)_{KN} = \left(\frac{r_0^2}{2}\right)\left(\frac{E_1}{E_0}\right)^2\left(\frac{E_1}{E_0}+\frac{E_0}{E_1}-2+4\cos^2\Theta\right),$$
(23a)

Θ being the angle between the electric vectors of the incident and scattered photons of energies E_0 and E_1, respectively. Averaged over polarizations, Eq. (23a) becomes

$$\left(\frac{d\sigma}{d\Omega}\right)_{KN} = \left(\frac{r_0^2}{2}\right)\left(\frac{E_1}{E_0}\right)^2\left(\frac{E_1}{E_0}+\frac{E_0}{E_1}-\sin^2\theta\right),$$
(23b)

where θ is the scattering angle. As might be expected, Eq. (23) results in integrals which are considerably more difficult to perform analytically. Since Monte Carlo techniques will easily determine whether use of the KN cross section will make a significant difference in multiple-scattering calculations, no analytic calculations employing Eq. (23) have been attempted. Again, for moderately thick samples, the isotropic results suggest that such differences are not likely to be large.

D. Variation of μ with energy

Our calculations have assumed that μ_1 and μ_2, the attenuation coefficients for one- and two-scattered photons, are equal to μ_0 for the incident photon. Since each scattering changes the photon energy by an amount depending upon the magnitude of the scattering angle, and since the variation of μ with energy is not, in general, insignificant,[17] our assumption of a single value of μ is not correct.

One may attempt to estimate the effect of this approximation by Monte Carlo calculations. Analytic calculations may attempt to minimize the effects of variation in μ by using an average μ for

the range of energies appropriate to a given experiment. More accurate results might be obtained by approximating μ as a linear function[2] of E:

$$\mu(E-E_0) \approx \mu_0 + b(E-E_0)$$

or, perhaps leading to more tractable integrals, by a relation of the form

$$\mu(E) \approx a/E^p.$$

Finally, we recall that the energy of the scattered photon depends [Eq. (4)] upon the electron momentum. Williams et al.[12] have analytically investigated this effect on the spectral distribution of doubly scattered photons, but incorporation of electron momentum into the present calculations of scattering probabilities and angular distributions would probably be exceedingly difficult.

E. Higher-order scattering

As Table V shows, triple and higher-order scattering are significant for infinite-radius samples even at small optical thickness. This rapid increase in multiple scattering with increasing ω appears to be an artifact of the infinite-radius geometry, since our own and other[5,7] Monte Carlo calculations on finite samples find considerably less higher-order scattering. For finite samples, escape of singly scattered photons through the sides of the cylinder will cut down the amount of multiple scattering. An upper bound on total multiple scattering is therefore given by

$$\sum_{n=2}^{\infty} P_n(\vec{V}) \leqslant \sum_{n=2}^{\infty} P_n^{\infty}(\omega) = 1 - e^{-\omega} - P_1^{\infty}(\omega).$$

For certain sample geometries, such as spherical, use of an isotropic cross section may make

TABLE V. Single, double, and higher-order scattering from infinite-radius cylinder as a function of optical thickness.

ω	$P_1^{\infty}(\omega)$	$P_2^{\infty}(\omega)$	$1-e^{-\omega}$ (Total scattering)	$\sum_3^{\infty} P_m^{\infty}(\omega)$
0.001	0.9964×10^{-3}	0.3107×10^{-5}	0.9995×10^{-3}	$<10^{-6}$
0.01	0.9725×10^{-2}	0.2192×10^{-3}	0.9950×10^{-2}	0.5966×10^{-5}
0.05	0.4473×10^{-1}	0.3633×10^{-2}	0.4877×10^{-1}	0.4070×10^{-3}
0.10	0.8186×10^{-1}	0.1106×10^{-1}	0.9516×10^{-1}	0.2243×10^{-2}
0.20	0.1399	0.3033×10^{-1}	0.1813	0.1104×10^{-1}
0.30	0.1821	0.5085×10^{-1}	0.2592	0.2623×10^{-1}
0.40	0.2127	0.7017×10^{-1}	0.3297	0.4681×10^{-1}
0.50	0.2347	0.8733×10^{-1}	0.3935	0.7144×10^{-1}
1.00	0.2715	0.1382	0.6321	0.2224
2.00	0.2369	0.1437	0.8647	0.4841
5.00	0.1738	0.9962×10^{-1}	0.9933	0.7198
10.00	0.1677	0.9243×10^{-1}	0.9995	0.7398

possible an analytic calculation of the probability of higher-order scattering. This does not appear to be the case here, since our difficulties in integration arise from the geometry rather than from the functional form of the cross section.

The results of astrophysicists[9,10,20] and of workers in neutron scattering[21] may shed some light on the problem of higher-order scattering. Monte Carlo calculations seem somewhat less attractive here, since they become less efficient as the number of scatterings increases.

VII. CONCLUSIONS

We have shown how multiple scattering varies with optical thickness in a simple model for a Compton-scattering experiment. Answers to the first question posed in Sec. I, to what extent are multiply scattered photons being observed, have been given for total scattering and for scattering at any fixed angle.

It has been found that for moderately large optical thickness, sample geometry rather than physics (differential scattering law) is the chief determinant of both the intensity and the angular distribution of multiple scattering. Answers to our second question, the effect of multiple scattering on the observed energy spectrum, will be presented in paper II.

ACKNOWLEDGMENTS

APPENDIX: SOME ASPECTS OF CYLINDER GEOMETRY

Consider an arbitrary point P in a cylinder of radius R_f and length t (see Fig. 4 for coordinate systems). We wish to find the distance from P to the cylinder boundary along some specified scattering direction (θ, φ). As seen in Fig. 10, for any P, the possible directions of scattering fall into three regions corresponding to escape through (I) the forward face, (II) the sides, and (III) the backward face. Let l be the distance from P to the cylinder boundary along (θ, φ). We shall first find l as a function of (θ, φ) in each of the three regions and then define the limits of the regions.

In region I, simple trigonometry gives

$$l = (t - z)/\cos\theta . \tag{A1}$$

For region III, we have simply

$$l = -z/\cos\theta . \tag{A2}$$

Region II is somewhat more complex. Consider a cross section C (Fig. 11) through the cylinder defined by a plane passing through P perpendicular to the z axis. Let $\vec{\rho}$ be the projection of the scattered path onto C, and let $\vec{r}$ be the vector in C from the z axis to P. The length of $\vec{\rho}$ is

$$\rho = l \sin\theta . \tag{A3}$$

From Fig. 11, it is evident that $|\vec{\rho} - \vec{r}| = R_f$, or, on squaring and solving for ρ,

$$\rho = r \cos\varphi + (R_f^2 - r^2 \sin^2\varphi)^{1/2} , \tag{A4}$$

where we have chosen the positive root of the quadratic since $\rho = r + R_f$ when $\varphi = 0$. Thus, combining (A3) and (A4), we have for region II

$$l = [r \cos\varphi + (R_f^2 - r^2 \sin^2\varphi)^{1/2}]/\sin\theta . \tag{A5}$$

The boundaries between the regions are defined by the heavy lines in Fig. 10, which trace out conical regions I and III when Fig. 10 is rotated about the z axis to produce the cylinder. The equation for the boundary between regions I and II is
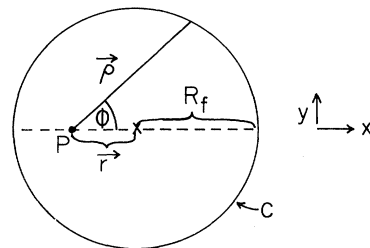

FIG. 10. Regions of scattering in a finite cylinder.

FIG. 11. Projection onto plane perpendicular to z axis of scattering from point P along (θ, φ). Cross represents z axis and $\vec{\rho}$ is projection of scattering direction onto plane.

$$\cos\theta^* = \frac{t-z}{l} = \frac{t-z}{[\rho^2 + (t-z)^2]^{1/2}}, \qquad (A6)$$

where ρ is given by Eq. (A4).

Similarly, the boundary between regions II and III is

$$\cos\theta^+ = -z/(\rho^2 + z^2)^{1/2}. \qquad (A7)$$

Thus, for $1 \geqslant \cos\theta > \cos\theta^*$, the scattering direction falls in region I, and l is determined by (A1). For $\cos\theta^* \geqslant \cos\theta \geqslant \cos\theta^+$, we are in region II, and the equation for l is (A5). Directions with $\cos\theta^+ > \cos\theta \geqslant -1$ lie in region III, for which l is given by (A2).

For our limiting geometry $(R_f - R_b \gg t)$, since $r < R_b$, (A4) reduces to $\rho \rightarrow R_f$ and we find that $\cos\theta^*$

$\rightarrow 0^+$ and $\cos\theta^+ \rightarrow 0^-$, according to (A6) and (A7).

The extension to higher-order scattering follows similar lines. For the double-scattering event described in Sec. V A, we find

$$l_3 = \begin{cases} (t - z_2)/\cos\theta_p, & 1 \geqslant \cos\theta_p \geqslant \cos\theta_p^*, \\ \rho_2/\sin\theta_p, & \cos\theta_p^* \geqslant \cos\theta_p \geqslant \cos\theta_p^+, \\ -z_2/\cos\theta_p, & \cos\theta_p^+ > \cos\theta_p \geqslant -1, \end{cases}$$

where

$$z_2 = z_1 + l_2' \cos\theta_1,$$

$$\rho_2 = -r_2 \cos\theta_p + (R_f^2 - r_2^2 \sin^2\theta_p)^{1/2},$$

and θ_p is the angle of observation. If $r \ll R_f$, then simple limiting values for ρ, $\cos\theta_p^*$, and $\cos\theta_p^+$ result as before.

---

*Work supported by the Camille and Henry Dreyfus Foundation.

[1]For recent reviews, see: (a) M. J. Cooper, Adv. Phys. 20, 453 (1971); (b) I. R. Epstein, Acc. Chem. Res. 6, 145 (1973); (c) International Review of Science, Ser. 2, Theoretical Chemistry, edited by A. D. Buckingham and C. A. Coulson (Butterworths, London, 1975); and (d) The Compton Effect, edited by B. G. Williams (McGraw-Hill, New York, to be published).

[2]B. G. Williams, Standardization of Compton Profile Measurements – The Compton Profile of Water, preliminary report, I. U. Cr. Commission on Charge, Spin and Momentum Density (University of Warwick, Coventry, England, 1974).

[3](a) J. W. M. Dumond, Phys. Rev. 36, 1685 (1930); (b) P. Kirkpatrick, Phys. Rev. 52, 1201 (1937).

[4]W. Lichtenberg and A. Przybylski, Nucl. Instrum. Methods 98, 99 (1972).

[5]J. Felsteiner, P. Pattison and M. Cooper, Philos. Mag. 30, 537 (1974).

[6]J. Felsteiner and P. Pattison, Nucl. Instrum. Methods 124, 449 (1975).

[7]B. G. Williams and V. Halonen, Phys. Fenn. 10, 5 (1975).

[8]W. R. McIntire, Phys. Status Solidi A23, 359 (1974).

[9]S. Chandrasekhar, Proc. R. Soc. A 192, 508 (1948).

[10]R. C. O'Rourke, Phys. Rev. 85, 881 (1952); 89, 999 (1953).

[11]P. J. Brockwell, Philos. Mag. 12, 515 (1965).

[12]B. G. Williams, P. Pattison, and M. J. Cooper, Philos. Mag. 30, 307 (1974).

[13]P. Pattison, S. Manninen, J. Felsteiner, and M. Cooper, Philos. Mag. 30, 973 (1974).

[14]A. C. Tanner, Thesis (Brandeis University, 1975) (unpublished).

[15]Such a cross section has in fact been used in the Boltzmann equation approach of Refs. 9 and 10 in order to render the equations more tractable.

[16]The notation $P_n^\infty(\omega, y)$ is used to signify the cumulative probability distribution, i.e., the probability that the photon scatters n times in a sample of optical thickness ω, then escapes with $y' < y$, where y' is an angle (e.g., θ) or a cosine (e.g., $x = \cos\theta$).

[17]The limiting ratio $(\omega \rightarrow \infty)$ of double-to-single scattering should be somewhat lower for a finite–radius cylinder; see, e.g., Ref. 7.

[18]Such quantities are tabulated in, e.g. J. H. Hubbell, Photon Cross Sections, Attenuation Coefficients, and Energy Absorption Coefficients from 10 keV to 100 GeV, Nat. Stand. Ref. Data Series, U.S.R.D.S.-N35 29 (U.S. GPO, Washington, D.C., 1969).

[19]J. D. Jackson, Classical Electrodynamics (Wiley, New York, 1962).

[20]S. Chandrasekhar, Radiation Transfer (Dover, New York, 1960).

[21]V. F. Sears, Adv. Phys. 24, 1 (1975).